GEOCARTO INTERNATIONAL
2025, VOL. 40, NO. 1, 2465446
https://doi.org/10.1080/10106049.2025.2465446

Taylor & Francis
Taylor & Francis Group

OPEN ACCESS Check for updates

A data-driven, cloud-based approach for forest aboveground biomass mapping using GEDI and other earth observation data: an ecoregion-specific Investigation across the state of Alabama, USA

Janaki Sandamali and Lana L. Narine

College of Forestry, Wildlife and Environment, Auburn University, Auburn, AL, USA

ABSTRACT
Forest aboveground biomass (AGB) is a crucial indicator for carbon monitoring. This study presents a data-driven, cloud-based workflow for AGB density (AGBD) mapping using Global Ecosystem Dynamics Investigation (GEDI) data combined with Earth observation (EO) datasets. Focusing on the state of Alabama, the specific objectives were to: (1) evaluate and compare the effectiveness of ecoregion-specific models versus a statewide model for estimating AGBD, and (2) generate a 30-m AGBD map based on the optimal model and assess agreement with forest inventory and global-scale information. GEDI data preparation was performed locally, while the analysis was conducted within GEE using the Random Forest algorithm. The ecoregion-specific models achieved higher accuracy (R^2: 0.20-0.71; RMSE: 66.67-48.99 Mg/ha) than the statewide model (R^2: 0.41; RMSE: 62.09 Mg/ha). These findings underscore the importance of ecoregion-specific modeling and combining EO data in cloud computing for advancing AGBD mapping.

ARTICLE HISTORY
Received 25 September 2024
Accepted 6 February 2025

KEYWORDS
Aboveground biomass; ecoregions; GEDI; Google Earth Engine; spaceborne lidar

1. Introduction

Forests play a crucial role in the Earth's carbon cycle, constituting around 30% of its total area and storing nearly 45% of its carbon reserves (Rodríguez-Veiga et al. 2017). Aboveground biomass (AGB) serves as a pivotal indicator for assessing forest carbon stocks (Yang et al. 2023). Forest of the Southern United States (US) stands out as comprising one of the world's most productive timberland systems (Shephard et al. 2022). Among them, Alabama holds the third-largest commercial forestland in the US with over 23 million acres of forestland covering almost 70% of the state and estimated to store approximately 1.16 billion metric tons of carbon (Duncan 2013; Adjei et al. 2023). Alabama's forests span six diverse level III ecoregions varied by climate and precipitation,

CONTACT Janaki Sandamali jsk0043@auburn.edu College of Forestry, Wildlife and Environment, Auburn University, Auburn, AL 36849, USA.

Supplemental data for this article can be accessed online at https://doi.org/10.1080/10106049.2025.2465446.

© 2025 The Author(s). Published by Informa UK Limited, trading as Taylor & Francis Group
This is an Open Access article distributed under the terms of the Creative Commons Attribution-NonCommercial License (http://creativecommons.org/licenses/by-nc/4.0/), which permits unrestricted non-commercial use, distribution, and reproduction in any medium, provided the original work is properly cited. The terms on which this article has been published allow the posting of the Accepted Manuscript in a repository by the author(s) or with their consent.

which influence forest productivity, species composition, and carbon storage capacity (Van Do et al. 2020; Commission for Environmental Cooperation (Montréal, Québec), & Secretariat 1997). Ecoregional variation plays a crucial role in determining the structure and function of forests and their contribution to carbon cycling. Studies conducted by Roitman et al. (2018) and Van Do et al. (2020) have demonstrated that forest biomass distribution and ecosystem functions vary significantly across ecoregions due to differences in environmental conditions.

AGB stands as a crucial indicator of carbon and its dynamic nature necessitates continuous measurement over time for accurate carbon estimation (Silva et al. 2021). Conventional field surveys provide accurate information but may be time-consuming, labor-intensive, and cost-prohibitive. Hence, remote sensing, and particularly spaceborne light detection and ranging (lidar), have emerged as powerful data sources for assessing forest structure and estimating AGB over large areas with remarkable details (Hummel et al. 2011; Harris et al. 2021; Nandy et al. 2021). The Global Ecosystem Dynamics Investigation (GEDI) is a spaceborne lidar instrument designed specifically to retrieve vegetation structure in comparison to other spaceborne lidar instruments (Dubayah et al. 2022a). Launched in 2018, GEDI, stationed on the International Space Station, offers measurements of forest vertical structure in temperate and tropical regions between 51.6° N and S latitude. GEDI offers both footprint and gridded products, encompassing raw and geolocated waveforms, footprint-level canopy height and profile metrics, gridded canopy height metrics and variability, along with footprint and gridded AGBD (Dubayah et al. 2020, 2022a; Kellner et al. 2022). The gridded AGBD GEDI Level 4B (GEDI L4B) is provided at a 1 km resolution, while the footprint AGBD GEDI Level 4 A (GEDI L4A) is provided with a 25 m diameter spaced and roughly 60 m along the track and approximately 600 m apart across the track. Previous studies have demonstrated the use of GEDI L4A data for generating mapped AGBD. For instance, Shendryk (2022) extrapolated GEDI L4A AGBD to create 100 m and 200 m AGBD maps for the United States and Australia and reported coefficient of determination (R^2) values ranging from 0.66 to 0.74, and root mean squared errors (RMSEs) of 55 to 81 Mg/ha. Similarly, Mohite et al. (2024) reported an R^2 of 0.64 and an RMSE of 46.59 Mg/ha for the Indian forest region at a 100 m resolution using GEDI L4A AGBD. Despite significant advancements in leveraging GEDI L4A data for mapping AGBD at various resolutions, there are limited approaches for generating 30 m resolution AGBD maps that explicitly consider GEDI L4A as the response variable, leveraging its unique characteristics as a spaceborne lidar-based sampling mission. Furthermore, studies tailored to ecoregion-specific approaches remain limited, specifically for temperate mixed forests of the southeastern United States. Furthermore, the potential of cloud computing platforms for efficiently processing large-scale GEDI datasets remains underexplored in this context. To address this gap, our study focuses on developing a framework to map AGBD at 30 m spatial resolution using GEDI L4A data within a cloud computing environment, incorporating an ecoregion-specific approach to improve accuracy and scalability.

Spaceborne lidar inherently faces challenges such as the lack of continuous spatial coverage. Therefore, fusion with other Earth Observation (EO) data enables the generation of continuous spatial coverage. Earlier studies that used spaceborne lidar data for AGB estimation concluded that a multi-sensor data fusion approach, leveraging the strengths of each mission, can produce wall-to-wall AGB information that is more accurate than what is achievable with any one sensor alone (Rodríguez-Veiga et al. 2017; Silva et al. 2021; Guerra-Hernández et al. 2022). In this study, we considered a range of EO data representing various portions of the electromagnetic spectrum, as suggested by previous studies, to represent an array of forest parameters. These datasets include Sentinel-1, Sentinel-2, Global 30 m digital elevation model (GLO30 DEM), Landsat 9, and Landscape Fire and Resource Management Planning Tools (LANDFIRE) data (Nandy et al. 2021; Guerra-Hernández et al. 2022). Landsat 9 is particularly noteworthy for its enhanced radiometric resolution, featuring 14-bit quantization for the Operational Land Imager-2 (OLI-2), an improvement from the 12-bit resolution of Landsat 8. This enhancement allows for more sensitive detection of subtle differences in dense forest areas (Kristi Sayler 2022). The decision to include Landsat 9 and LANDFIRE data in our analysis was driven by the limited number of studies that have explored the utility of Landsat 9 for AGB estimation. Additionally, to our knowledge, no studies have integrated LANDFIRE data in conjunction with Landsat 9 for AGBD mapping. This integration presents a unique and valuable aspect of our investigation.

Analysis with spaceborne lidar requires managing substantial and increasingly voluminous datasets, such as the billions of forest structural data sampler points provided by GEDI across the tropics (Holcomb et al. 2023). Integrating spaceborne lidar with other EO data, especially for larger areas, necessitates the management of extensive and growing volumes of lidar data (Béjar-Martos et al. 2022). Google Earth Engine (GEE) has emerged as a viable platform for this purpose, offering a comprehensive framework for effectively managing, sharing, and modeling spatial data (Gorelick et al. 2017; Kacic et al. 2021).

Considering the complexities of spectral variation within land cover classes and the challenges of per-pixel classification, a 30 m grid size has emerged as the preferred spatial resolution (Giri et al. 2013). This resolution effectively captures diverse features on Earth's surface while maintaining a balance between detail and coverage (Chen et al. 2015). Furthermore, when conducting regional and global-scale mapping, most existing data products are available at a 30 m resolution (e.g. Landsat 9, GLO-30 DEM, LANDFIRE data). This makes it compatible with widely used datasets and provides flexibility for integration and utilization in various applications (Townshend et al. 2012; Giri et al. 2013; Hansen et al. 2013). In addition, when conducting regional-scale AGBD estimation, it is crucial to consider the inherent characteristics of the vegetation of the region (Roitman et al. 2018). As highlighted by the Commission for Environmental Cooperation report in 1997, ecoregions play a vital role in shaping regional environmental management assessments, reporting, and decision-making processes. Level III ecoregions, being smaller in scale, enable the identification of local characteristics and the formulation of more specifically oriented management strategies. However, no previous studies have investigated the use of GEDI for ecoregion-specific AGBD mapping using cloud computing in a regional context. Therefore, this study introduces a novel approach to employing spaceborne lidar data for ecoregion-based AGBD estimation in GEE.

Existing AGB products, such as those from the US Forest Service's Forest Inventory and Analysis (FIA) program (Gray et al. 2012), GEDI L4B AGBD (Dubayah et al. 2023), and the European Space Agency's (ESA) Climate Change Initiative (CCI) (Santoro and Cartus 2023), provide valuable AGB estimates at both plot-level and global scales. However, these products are often constrained by limitations in spatial resolution, integration of ecoregion-specific approaches, and spatially comprehensive coverage; factors that are critical for localized forest management and conservation planning. The primary goal of this study is to develop a data-driven, cloud-based workflow for AGBD mapping using GEDI footprint AGBD and EO data. Focusing on the state of Alabama, the specific objectives were to: (1) evaluate and compare the effectiveness of ecoregion-specific models versus a generalized statewide model for estimating AGBD, and (2) generate a 30-m statewide AGBD map based on the optimal model and assess agreement with FIA and CCI data.

2. Methodology

The methodology entails collecting AGBD footprints from GEDI L4A, integrating multi-source EO data, and conducting analysis in GEE (Figure 1). A variety of predictor variables were utilized for AGBD estimation, including datasets from Sentinel-1, Sentinel-2, Landsat 9, GLO 30 DEM derivatives, LANDFIRE, and National Land Cover Dataset (NLCD). Two modeling approaches were evaluated: a generalized statewide model and ecoregion-specific models tailored to individual regions. Both models were trained using the RF machine learning algorithm, and model accuracy was assessed using holdout test data. Additionally, the mapped AGBD product was compared with available county-level and global-scale AGB datasets to evaluate its accuracy further.

2.1. Study area

The state of Alabama, situated in the southeastern US between 30° and 35° north latitude and 85° to 88.5° west longitude, covers a total area of approximately 135,767 km^2 (Figure 2). Alabama boasts a diverse landscape, including mountains, mixed forests, and coastal plains. The predominant land use in the state is timberlands, constituting 71% of the total land area (Adjei et al. 2023). Covering 23.03 million acres, Alabama's timberlands represent the third-largest commercial forestland in the United States. Forests in Alabama provide critical ecosystem services, including carbon sequestration, enhancement of air and water quality, and support for biodiversity (Chen 2010). This area includes

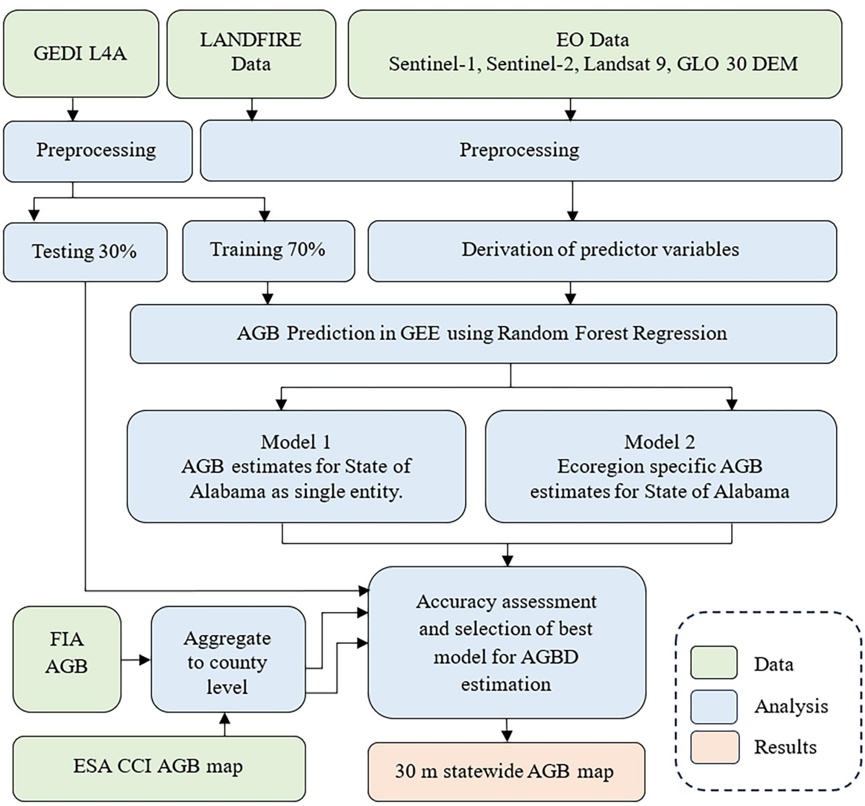

Figure 1. The workflow adopted in experimental analysis.

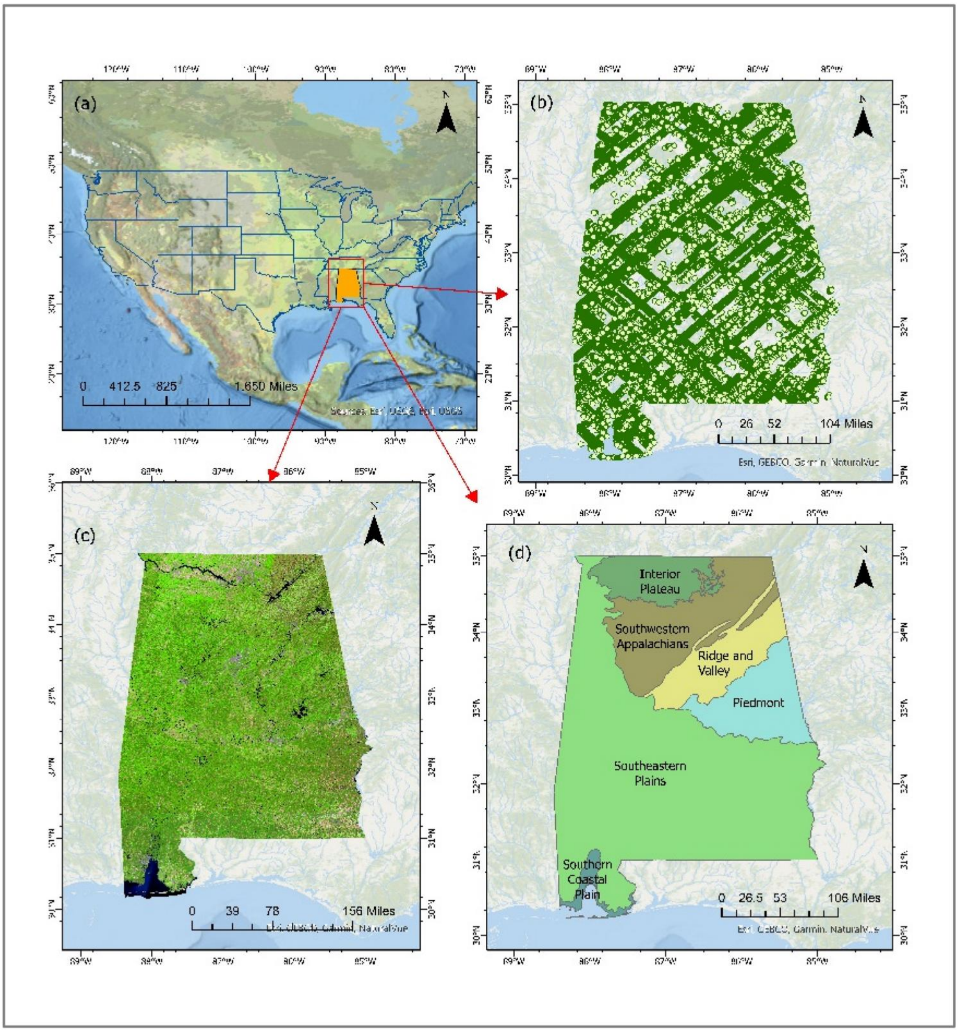

Figure 2. Study area of the investigation. (a) The spatial location of the state of Alabama concerning the United States, (b) GEDI L4A footprint AGBD data, (c) landsat 9 false color (vegetative analysis) composite image (bands: short-wave infrared (SWIR)-1, near infra-red (NIR), red), and (d) level III ecoregions of the study area.

National Wildlife Refuges, designated Wilderness Areas, and commercial forest lands by underscoring these forests' ecological and economic significance (Alabama Forest Commission 2023). The state is home to four national forests: William B. Bankhead National Forest, Talladega National Forest (consisting of two tracts), Tuskegee National Forest, and Conecuh National Forest (Hartsell and Cooper 2013). Ownership of Alabama's forests is predominantly private, with approximately 93.4% of timberlands under private ownership and only 6.6% publicly owned. The forest composition is characterized by a mix of softwood and hardwood species, with softwoods, primarily pines, accounting for 47% of the timberland, hardwoods 41%, and mixed hardwood/pine stands 12% (Alabama Forest Commission 2023). The loblolly-shortleaf pine forest type dominates, covering 39% or roughly 9.0 million acres of forestland. Loblolly pine, the most prevalent softwood species, constitutes nearly 80% of the state's live softwood volume, with an estimated 14 billion cubic feet of growing stock. The biophysical productivity of

Alabama's forests is significant, with annual net growth rates of 54.9 million tons for softwoods and 21.2 million tons for hardwoods (Alabama Forest Commission 2023).

Alabama experiences a climate characterized by mild winters, hot summers, and consistent year-round precipitation. Renowned for its rich biodiversity, Alabama stands as one of the most ecologically diverse states in the United States, serving as a global hotspot for various plants and animal species (Duncan 2013). The ecological composition of Alabama is categorized into six level III ecoregions: interior plateau, southwestern Appalachians, piedmont, southeastern plains, southern coastal plain, and ridge and valley as depicted in Figure 2d (USFWI 2024).

2.2. Data

The data employed in the study included open-access EO data obtained from various sources, including the Oak Ridge National Laboratory Distributed Active Archive Centre (ORNL DAAC), NASA Earth data platform, GEE catalog, LANDFIRE web portal, and Earth Resources Observation and Science Center.

2.2.1. GEDI L4A footprint level Aboveground biomass density data

Previous studies utilizing GEDI L4A as the response variable incorporated one year of data for AGB estimation (Shendryk 2022; Mohite et al. 2024). Annual satellite data ensures consistency in environmental conditions, reduces the influence of inter-annual variability, and captures the annual phenological cycle, which is crucial for accurate AGB estimation (Zhang et al. 2003; Soudani et al. 2021). Hence, to map AGB for the year 2022, we acquired GEDI L4A from January 1, 2022, to December 31, 2022. A comprehensive data filtering process was conducted, guided by GEDI quality filters and previous studies, with a total of seven filters applied (Liu et al. 2021; Dubayah et al. 2022a; Shendryk 2022; Bruening et al. 2023). Initially, data not meeting Level 4 A quality requirements were excluded using the 'l4_quality_flag'. Subsequently, a beam sensitivity threshold of 0.98 was applied by considering Alabama's mixed forest characteristics, aiming to minimize measurement error in relative height metrics (Dubayah et al. 2022a; Indirabai and Nilsson 2024). Further refinement involved the removal of unreliable GEDI measurements which exhibited more than 50% relative standard error as shown by Shendryk (2022). Additionally, GEDI measurements on slopes greater than 30 degrees were excluded, as prior findings indicated their adverse impact on the accurate retrieval of both terrain and tree heights (Liu et al. 2021). Then, GEDI measurements exclusively from the full power beams ('BEAM0101', 'BEAM0110', 'BEAM1000', and 'BEAM1011'), specifically designed for dense vegetation, were selected (Liu et al. 2021). Furthermore, GEDI data acquired during nighttime (solar elevation < 0) were utilized to mitigate the background solar illumination since waveform quality is compromised during daytime due to the impact of solar interference (Liu et al. 2021; Shendryk 2022). Out of all available GEDI measurements (592,184), 117, 016 remained after the data filtering for further processing (Figure 3) before masking to forest areas. In addition, GEDI data within unsuitable land cover and land use categories (e.g. built-up areas, barren lands, shrub/scrub, grasslands, etc.) were excluded based on the National Land Cover Database (NLCD), retaining only forested areas for the analysis. The selected NLCD land cover classes included 41 (deciduous forest), 42 (evergreen forest), 43 (mixed forest), and 90 (woody wetlands) (Shendryk 2022).

The distribution of GEDI L4A AGBD exhibited significant skewness as depicted in Figure 4a. To prepare the data for analysis, various transformations were explored, including box cox (Atkinson et al. 2021), inverse (Ross 2013), logarithmic (Leydesdorff and

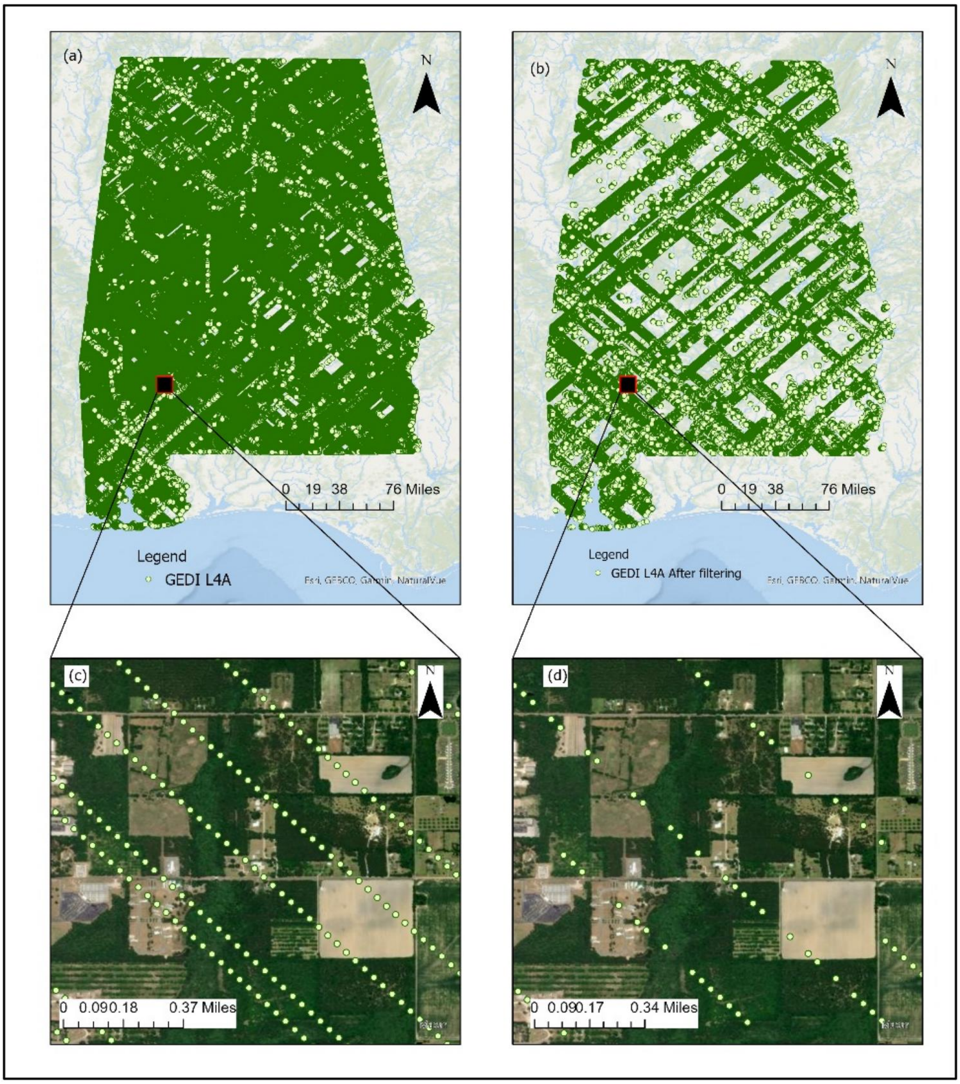

Figure 3. GEDI footprints over the state of Alabama for 2022 (a) before filtering, (b) after filtering and before masking to Forest areas, (c) zoomed-in area showing the distribution of GEDI data over the selected study site before filtering, (d) the same zoomed-in area after filtering and before masking to Forest areas.

Bensman 2006), and square root transformations (Gregoire et al. 2008) in the python environment. The square root transformation was selected, as it rendered the distribution closer to a normal Gaussian distribution, enhancing the model's predictive accuracy and reducing bias (Shendryk 2022). Subsequently, the transformed data was uploaded to GEE for further analysis, serving as the response variable in the model.

2.2.2. Mapped Earth Observation predictors

Predictor variables used for upscaling footprint-level AGBD are listed in Table 1. Variables considered are deemed important in mapping AGB and forest structural parameters according to earlier literature (Li et al. 2020; Nandy et al. 2021; Guerra-Hernández et al. 2022; Jiang et al. 2022; Malambo et al. 2023; Moradi et al. 2022; Shendryk 2022; Tiwari and Narine 2022; Dewitz 2023; Franks and Rengarajan 2023; La Puma 2023).

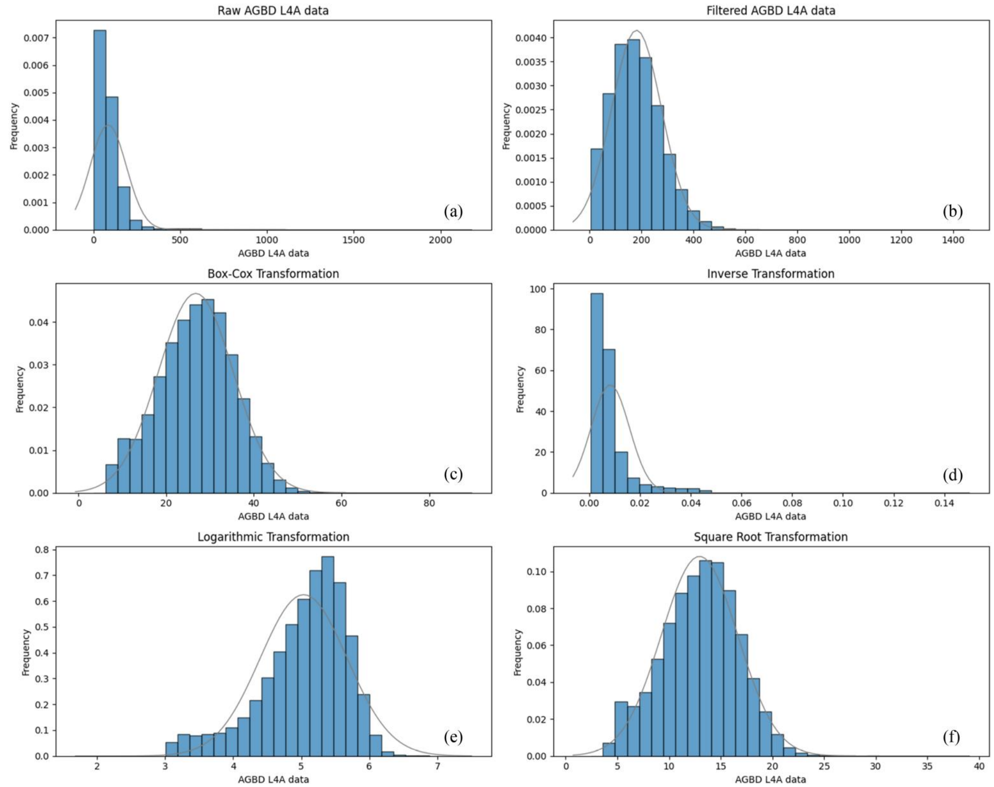

Figure 4. Frequency distribution of GEDI L4A (a) the raw AGBD data, (b) filtered AGBD after applying filters to remove unsuitable erroneous footprint AGB, (c) Box-Cox transformation, (d) inverse transformation, (e) logarithmic transformation, (f) square root transformation.

2.2.2.1. Sentinel-1. The Sentinel-1 satellites collect C-band SAR, utilizing the Interferometric Wide Swath mode with VV (Vertical transmit - Vertical receive) and VH (Vertical transmit - Horizontal receive) polarizations, yielding Multi-Look Ground Range-Detected products (ESA, 2012; Laurin et al. 2018). All available Sentinel-1 images from January to December 2022 were utilized in this study, sourced from the 'COPERNICUS/S1_GRD' Sentinel-1 image collection within the GEE. These images were processed to backscatter coefficient (σ°) in decibels (dB). For analysis, Sentinel-1 imagery was composited by computing the median of each band from all ascending orbit images at a spatial resolution of 30 m, and then mosaicked to cover the extent of Alabama. Additionally, band ratios (VV/VH) and band differences (VV - VH) were calculated, as they have demonstrated efficacy in forest-related studies, along with the VV and VH bands (Soudani et al. 2021). As shown by Chen et al. (2019) the texture features from Sentinel −1 data were more suitable for AGB estimation. Therefore, our study derived a range of textures from the Grey Level Co-occurrence Matrix (GLCM) using both VV and VH polarizations.

2.2.2.2. Sentinel-2. The Sentinel-2 data accessible in the GEE platform was obtained from Scihub and processed using the Sen2Cor which is a processor for Sentinel-2 Level 2 A product generation and formatting (ESA 2022). The study incorporated Sentinel data spanning from January 2022 to December 2022. Initially, atmospheric corrections were applied while simultaneously masking out clouds and cloud shadows from all images. This was achieved by utilizing the QA60 band, which contains quality assessment data,

Table 1. Data sources and variables are incorporated in the study for Forest AGB estimation.

No	Source	Variables	References
01	Sentinel-1	VV / VH band ratios (VV/VH) band differences (VV - VH) Textures angular second moment, contrast, correlation, dissimilarity, entropy, variance, difference entropy, difference variance.	(Li et al. 2020; Nandy et al. 2021; Guerra-Hernández et al. 2022)
02	Sentinel-2 / Landsat 9	Spectral bands: NIR / Red / Green / Blue / rededge1 / rededge2 / rededge3 / rededge4 / SWIR1 / SWIR2 Vegetation Indices: Normalized Difference Vegetation Index (NDVI) / Soil Adjusted Vegetation Index (SAVI) / Simple Ratio Vegetation Index (SR) / Optimized Soil Adjusted Vegetation Index (OSA) / Green Normalized Difference Vegetation Index (GNDVI) / Modified Soil Adjusted Vegetation Index (MSAVI) / green Chlorophyll Index (CI green)	(Jiang et al. 2022; Moradi et al. 2022; Shendryk 2022)
03	GLO30 DEM	DEM / Slope / Aspect	(Franks and Rengarajan 2023)
04	LANDFIRE Data	Canopy Bulk Density (CBD), Canopy Base Height (CBH), Canopy Cover (CC), Canopy Height (CH), Existing Vegetation Cover (EVC), and Existing Vegetation Height (EVH)	(Malambo et al. 2023; La Puma 2023)
05	NLCD Data	Land cover / Tree canopy cover	(Tiwari and Narine 2022; Dewitz 2023)

including information on cloud and cirrus presence. Bit 10 of the QA60 band evaluates cloud presence (0: absent, 1: present), while bit 11 assesses cirrus presence (0: absent, 1: present). Subsequently, bit masks for cloud and cirrus were detected and applied to mask out corresponding areas from the images. Data filtering was then performed, retaining only images with a cloud pixel percentage of less than five. Following this, all images were composited by computing the median of all cloud and cloud shadow-masked images, with the resultant resolution set at 30 m (Shendryk 2022). Moreover, Sentinel-2 imagery was employed to derive vegetation indices (Table 2), which have previously shown effectiveness on AGB estimation, as illustrated in Table 1.

2.2.2.3. Landsat 9. Data from Landsat 9, accessible through the GEE, provides atmospherically corrected surface reflectance and land surface temperature measurements derived from OLI/TIRS sensors. Landsat 9 includes 11 spectral bands, ranging from visible to thermal infrared (Masek et al. 2020). For this study, we specifically used the Blue, Green, Red, NIR, SWIR1, and SWIR2 bands, which are typically used for vegetation analysis (USGS 2024). These bands were selected for their ability to capture relevant surface and vegetation characteristics (Table 1) (Jiang et al. 2022). For our study, Landsat 9 images from January to December 2022 in Collection 2, Tier 1, Level 2 data were utilized, following additional processing to enhance geometric and radiometric accuracy. Cloud masking based on 'QA_PIXEL' values was applied, followed by filtering to retain images with less than five percent cloud cover. The images were then sorted in descending order to prioritize recent acquisitions, culminating in the computation of a median composite. Furthermore, Landsat 9 imagery was utilized to derive vegetation indices (Table 2), which have previously shown significant impacts on AGB estimation.

Table 2. Vegetation indices used for AGBD estimation.

Vegetation index	Equation	References
CI green	$\text{CI green} = \frac{(\text{NIR})}{(\text{GREEN})} - 1$	(Gitelson et al. 2005)
GNDVI	$\text{GNDVI} = \frac{(\text{NIR-GREEN})}{(\text{NIR+GREEN})}$	(Gitelson and Merzlyak 1998)
MSAVI	$\text{MSAVI} = \frac{\left(2\text{NIR}+1-((2\text{NIR}+1)^2-8(\text{NIR-RED}))^{1/2}\right)}{(2)}$	(Qi et al. 1994)
NDVI	$\text{NDVI} = \frac{(\text{NIR-RED})}{(\text{NIR+RED})}$	(Rouse et al. 1974)
OSA	$\text{OSA} = 1.6\left(\frac{(\text{NIR-RED})}{(\text{NIR+RED+0.16})}\right)$	Rondeaux et al. (1996)
SR	$\text{SR} = \frac{(\text{NIR})}{(\text{RED})}$	(Jordan 1969)
SAVI	$\text{SAVI} = 1.5\left(\frac{(\text{NIR-RED})}{(\text{NIR+RED+0.5})}\right)$	Huete (1988)

2.2.2.4. GLO30 DEM. The GLO30 DEM, extracted from WorldDEM data acquired between 2011 and 2015, is publicly accessible *via* GEE and was subset to Alabama. Subsequently, slope and aspect calculations were performed to serve as predictor variables for the analysis (Franks and Rengarajan 2023). The GLO30 DEM has been successfully utilized in previous AGB studies, demonstrating its reliability and applicability (Shendryk 2022). It has also served as a significant contributor to global AGB estimation studies, such as the ESA CCI AGB mapping (Santoro and Cartus 2023) and the PlanetScope Carbon Monitoring-AGB product (Planet Labs 2024).

2.2.3. Other ancillary data

2.2.3.1. LANDFIRE data. LANDFIRE is an interagency initiative aimed at providing comprehensive biological, ecological, and geospatial data and databases covering the contiguous United States, Alaska, Hawaii, and insular areas (La Puma 2023). It offers consistent and detailed maps and data delineating vegetation, wildland fuel, fire regimes, and ecological deviation from historical norms across the nation at a 30 m resolution. This study utilizes CBD, CBH, CC, CH, EVC, and EVH all of which are appropriate to biomass and forest parameters as illustrated in Table 1 (Malambo et al. 2023). La Puma 2023;

2.2.3.2. NLCD land cover and tree canopy datasets. The NLCD serves as an operational program for monitoring land cover in the United States, offering updated information spanning from 2001 to the present (Dewitz 2023). In our study, we utilized the NLCD 2021 land cover and tree canopy cover products from the U.S. Forest Service as independent predictor variables in our estimation of AGBD (Tiwari and Narine 2022; Dewitz 2023).

2.3. Extrapolation of GEDI L4A AGBD

The extrapolation of GEDI L4A AGBD involves the collection of footprints AGBD from GEDI L4A, integration of multisource EO data, and performance analysis in GEE. A total of sixty predictor variables, sourced from various platforms, were employed for estimating AGBD. These variables include 19 from Sentinel-1 derivatives, 18 from Sentinel-2, 13 from Landsat 9, three from GLO 30 DEM derivatives, six from the LANDFIRE program, and one from NLCD land cover. The study aimed to map AGBD for the entirety of 2022. However, the available GEDI Version 2.1 Level 4 A footprint-level AGBD datasets in GEE provided temporal coverage only until June 9, 2022, which posed potential temporal inconsistencies in the analysis. While the rasterized version of the L4A data in GEE offered a convenient alternative, we prioritized the use of footprint-level AGBD data to align with the study's objectives. To address these limitations, GEDI L4A data was downloaded from NASA's Earth data platform, preprocessed locally, and subsequently uploaded to GEE for RF model execution and analysis.

To estimate AGBD, we utilized the RF machine learning algorithm, which has proven to be both effective and computationally efficient for handling large volumes of remote sensing data (Almeida et al. 2019). Further, the RF algorithm has become a popular tool in remote sensing due to its robustness to multicollinearity, noise, outliers, and overfitting, as well as its strong predictive capabilities for high-dimensional datasets (Belgiu and Drăguț 2016). Previous studies underscored the advantage of the RF model for AGB mapping as a robust machine-learning technique with remote sensing data (Narine et al. 2019; Su et al. 2020; Nandy et al. 2021). For instance, Wang et al. (2018) investigated the effectiveness of different techniques for AGB mapping in Maryland, including a principal components model, backpropagation artificial neural network, support vector regression (SVR), and RF. The study found that machine learning methods outperformed the principal components model, with the RF model performing the best, achieving an R^2 of 0.70 and RMSE of 35.81 Mg/ha. Similarly, Xu et al. (2023) compared multiple linear regression (MLR), SVR, and RF for mapping AGB in Quercus Forest in the alpine mountains of Yunnan Province, China. The study revealed that the RF model provided the most accurate results, with an R^2 of 0.91 and RMSE of 17.93 Mg/ha, outperforming the MLR and SVR models. In addition to these studies, several other researchers, such as Zhang et al. (2014), Shen et al. (2018), and Wang et al. (2024) have compared a range of models for AGB mapping in different parts of the world. These studies have consistently concluded that the RF model outperforms the other models in terms of accuracy and reliability for AGB mapping. Moreover, RF has shown robustness against noise in training samples (Su et al. 2020), further solidifying its applicability in AGB mapping in this study. RF operates as an ensemble learning method that builds multiple decision trees during training and combines their outputs to improve prediction accuracy and reduce overfitting (Freeman et al. 2018). A study conducted by Li et al. (2020) showed that extensive hyperparameter tuning does not always yield significant accuracy improvements in RF modeling for AGB mapping when compared with other machine-learning approaches. RF is robust due to its relatively few user-set parameters and it is less sensitive to extensive hyperparameter tuning (Freeman et al. 2018). Thus, we employed a 'model-as-is' approach for this study, utilizing all predictor variables and the default hyperparameters provided by GEE.

GEDI data preprocessing and preparation were conducted locally, and processed data, along with other datasets not available in GEE, were manually uploaded to the platform. Once the data were loaded into GEE, metadata was reviewed, parameters adjusted, and the RF model developed. The AGBD extrapolation was subsequently performed entirely within GEE at a 30 m spatial resolution. To compare ecoregion-specific AGB mapping, we tested two modeling approaches: (1) a statewide model treating the entire study area as a single entity (referred to as Model 1) and (2) ecoregion-specific models developed individually for each of the six ecoregions (referred to as Model 2). For model training and testing, the data were partitioned into 70% for training and 30% for testing. Finally, the mapped outputs were downloaded to a local machine, and map preparation and visualization were conducted using ArcGIS Pro (Esri, 2024).

2.4. Accuracy assessment

To evaluate the accuracy of the AGB estimates derived from our models, we employed a set of statistical metrics, including (i) the Pearson correlation coefficient (r), (ii) bias, (iii) relative bias (rbias), (iv) the coefficient of determination (R^2), (v). the root-mean-square error (RMSE), (vi) mean absolute percentage error (MAPE), and (vii) percentage accuracy (PA).

$$r = \frac{\sum_{i=1}^{n}(x_i - \overline{x})(y_i - \overline{y})}{\sqrt{\sum_{i=1}^{n}(x_i - \overline{x})^2 \sum_{i=1}^{n}(y_i - \overline{y})^2}} \tag{1}$$

$$\text{bias} = \frac{1}{n}\sum_{i=1}^{n} (\hat{y} - y_i) \tag{2}$$

$$\text{rbias} = \left(\frac{\text{Bias}}{\overline{y}}\right) 100\% \tag{3}$$

$$R^2 = 1 - \frac{\sum_{i=1}^{n}(\overline{y} - y_i)^2}{\sum_{i=1}^{n}(y_i - \overline{y})^2} \tag{4}$$

$$RMSE = \sqrt{\frac{1}{n}\sum_{i=1}^{n} (\overline{y} - y_i)^2} \tag{5}$$

$$\text{MAPE} = \frac{1}{n}\sum_{i=1}^{n} \left(\frac{y_i - \overline{y}}{y_i}\right).100 \tag{6}$$

$$\text{PA} = 100 - MAPE \tag{7}$$

Where x_i *and* y_i are the observed values, $\hat{y}$ are the predicted values, $\overline{x}$ *and* $\overline{y}$ is the mean of the observed values, k is the number of predictors or independent variables, and n is the number of observations.

2.5. Assessment of statewide AGBD map

The ecoregion-specific AGBD map (30-meter spatial resolution) generated by this study using GEDI L4A was compared with two other AGBD data sources: the Forest Inventory and Analysis (FIA) plot-level AGBD data (provided as plot-level AGBD estimates with associated coordinates and positional uncertainty) (Gray et al. 2012), and the ESA CCI AGBD product, available at a 100-meter spatial resolution (Santoro and Cartus 2023).

Initially, we employed data obtained from the FIA program, spanning from 2013 to 2023, to minimize the temporal gap between estimated AGBD maps and FIA measurements. However, due to ecological integrity and security concerns, the accurate locations of these plots are displaced by approximately one mile, making direct assessment of AGBD impractical. Consequently, we aggregated FIA plot data by computing the average AGBD at the county level for comparison. We then compared this county-level aggregated FIA with the average AGBD derived from our study, which was masked to forests (NLCD classes: deciduous forest, evergreen forest, mixed forest, and woody wetland) based on the 2021 NLCD (Dewitz 2023). It is important to note that the 'FIA AGBD ' referred to here is not a pre-existing product, but an aggregated dataset created specifically for this study. Additionally, we utilized the most recent globally available ESA CCI AGBD dataset from 2020 as a secondary reference for comparison (Shendryk 2022; Hunka et al. 2023; Bhat et al. 2024). The CCI map was masked to the geographic extent of the state of Alabama and re-projected to a uniform frame of reference (NAD 1983 Albers Contiguous USA). We selected forest-only pixels by adhering to the CCI and NLCD guidelines, aggregated the CCI data to the county level, and compared estimates with the county-level aggregated predicted forest AGB from this study.

3. Results

3.1. Comparison of GEDI-derived AGBD from ecoregion-specific and statewide models

As depicted in Figure 5, the accuracy metrics produced using withheld test data indicate superior performance of model 2 (r: 0.46 – 0.87, rbias: −5.73% - −3.24%, R^2: 0.20 – 0.71, and RMSE: 66.67 Mg/ha – 48.99 Mg/ha) compared to model 1 (r: 0.64, rbias: −3.86%, R^2: 0.41, and RMSE: 62.09 Mg/ha). Notably, the model 2 exhibited varied R^2 and RMSE values across different ecoregions, with the southern coastal region showing suboptimal performance (r: 0.46, rbias: −5.73%), primarily attributed to insufficient number of samples (n) for analysis and the inherent characteristics of the land cover which includes estuaries, salt marshes, lagoons, bayous, river deltas, and wetlands (Bouasria et al. 2023; USFWI 2024).

We observed that all models experienced both overestimation and underestimation. Specifically, as depicted in Figure 5, the predicted AGBD values tended to be higher than the actual values when AGBD was low (AGBD $\leq$ 100 Mg/ha) and lower than the actual values when AGBD was high (AGBD $\geq$ 300 Mg/ha). This pattern indicates that, despite leveraging multi-sensor dataset synergy to minimize estimation errors, the models still overestimate AGBD at lower values and underestimate it at higher values. These discrepancies, characterized by overestimation at low AGBD and underestimation at high AGBD, are consistent with findings from other studies utilizing GEDI (e.g. Shendryk (2022), Jia et al. (2023), Dong et al. (2023), and Lutz et al. (2024)). In sparsely vegetated regions, predictor variables such as spectral reflectance or terrain metrics may suggest the potential presence of biomass, leading to small positive biomass predictions even when GEDI reports zero biomass. Additionally, GEDI's lidar signals often saturate dense forests, limiting sensitivity to high biomass values and contributing to underestimation in regions with high AGBD (Li et al. 2024). These trends highlight challenges in model generalization in low-biomass regions, saturation effects in high-biomass areas, and persistent biases in the training data. Such observations underscore the inherent complexities of biomass estimation using GEDI data and machine-learning techniques.

The relative variable importance graph highlighted the predictors' effect on model enhancement across the six ecoregions. We generated six separate variable importance graphs using GEE and, for better representation, combined them into a single variable importance graph using Python, as shown in Figure 6. The results revealed that variables from the LANDFIRE program outperformed other predictors, underscoring the significance of LANDFIRE data in AGBD estimation. Their consistently high importance across all ecoregions suggests that land cover and vegetation-related features, particularly LANDFIRE data, provide critical contextual information that improves AGBD model predictions by refining biomass characterization at regional scales. The LANDFIRE layers are developed using predictive landscape models that integrate field-based measurements, satellite imagery, and biophysical gradient data through classification and regression tree techniques (La Puma 2023). Among these layers, the most influential predictor in this analysis is the EVC and EVH. EVC quantifies the vertical projection of live canopy cover at a 30 m resolution and provides estimates for different vegetation types, including trees, shrubs, and herbaceous cover. Further, EVH represents the average height of the dominant vegetation for a 30 m spatial resolution. These estimates are derived using a combination of ground-based visual assessments at plot levels, lidar-derived canopy observations, and spatially explicit geospatial layers (Rollins 2009). Furthermore, previous studies have demonstrated the value of integrating LANDFIRE data with remote sensing-derived predictors for forest-related analyses (Malambo et al. 2023). Additionally, variables such as

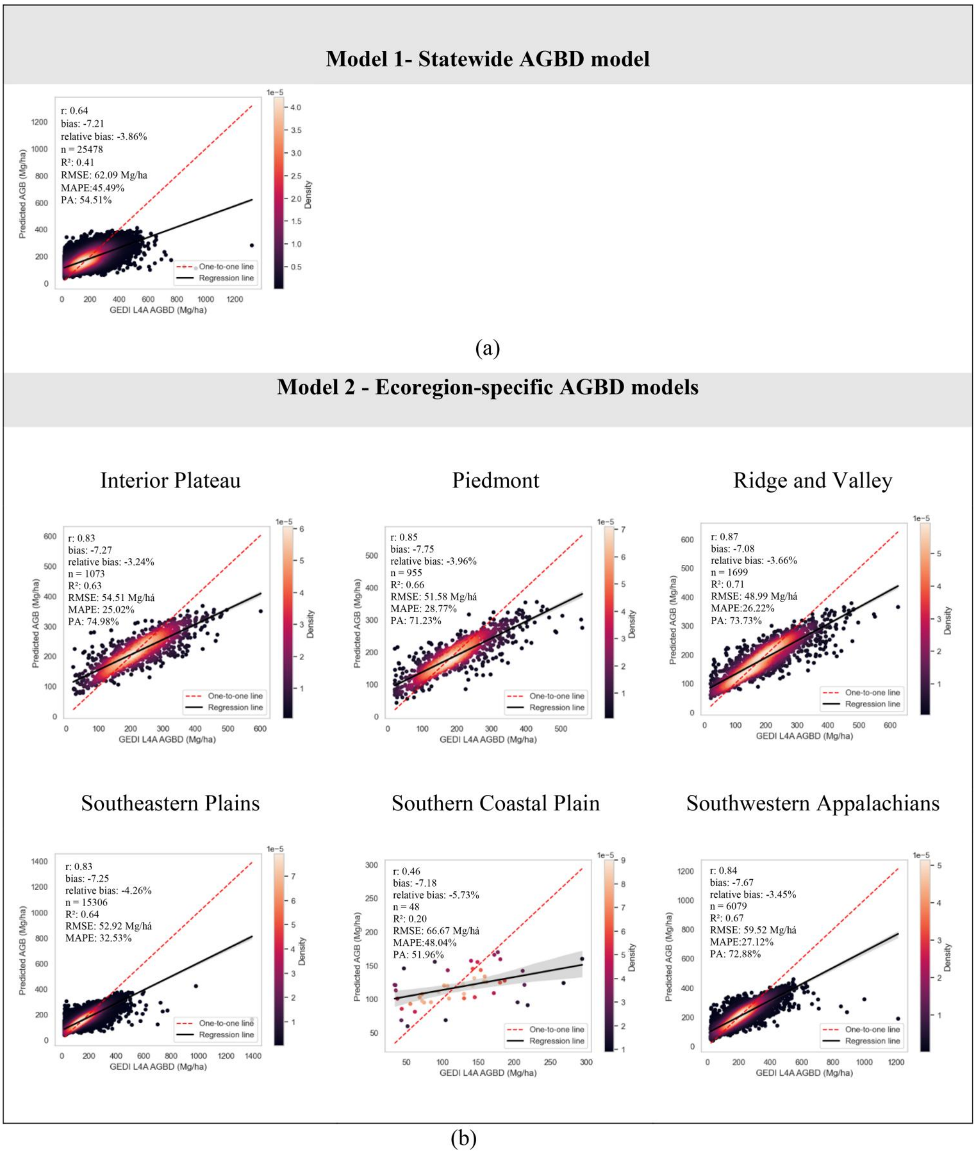

Figure 5. Scatter plot of estimated vs withhold AGBD in Mg/ha (a) performance of model 1. And (b) the performance of model 2.

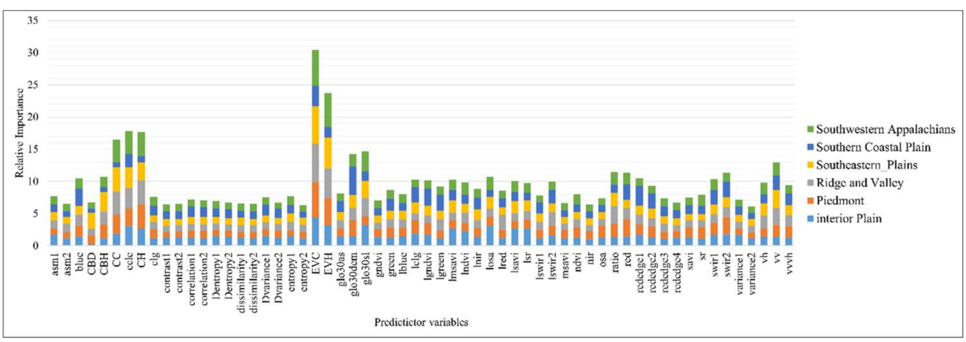

Figure 6. Variable importance at each ecoregion for all predictor variables.

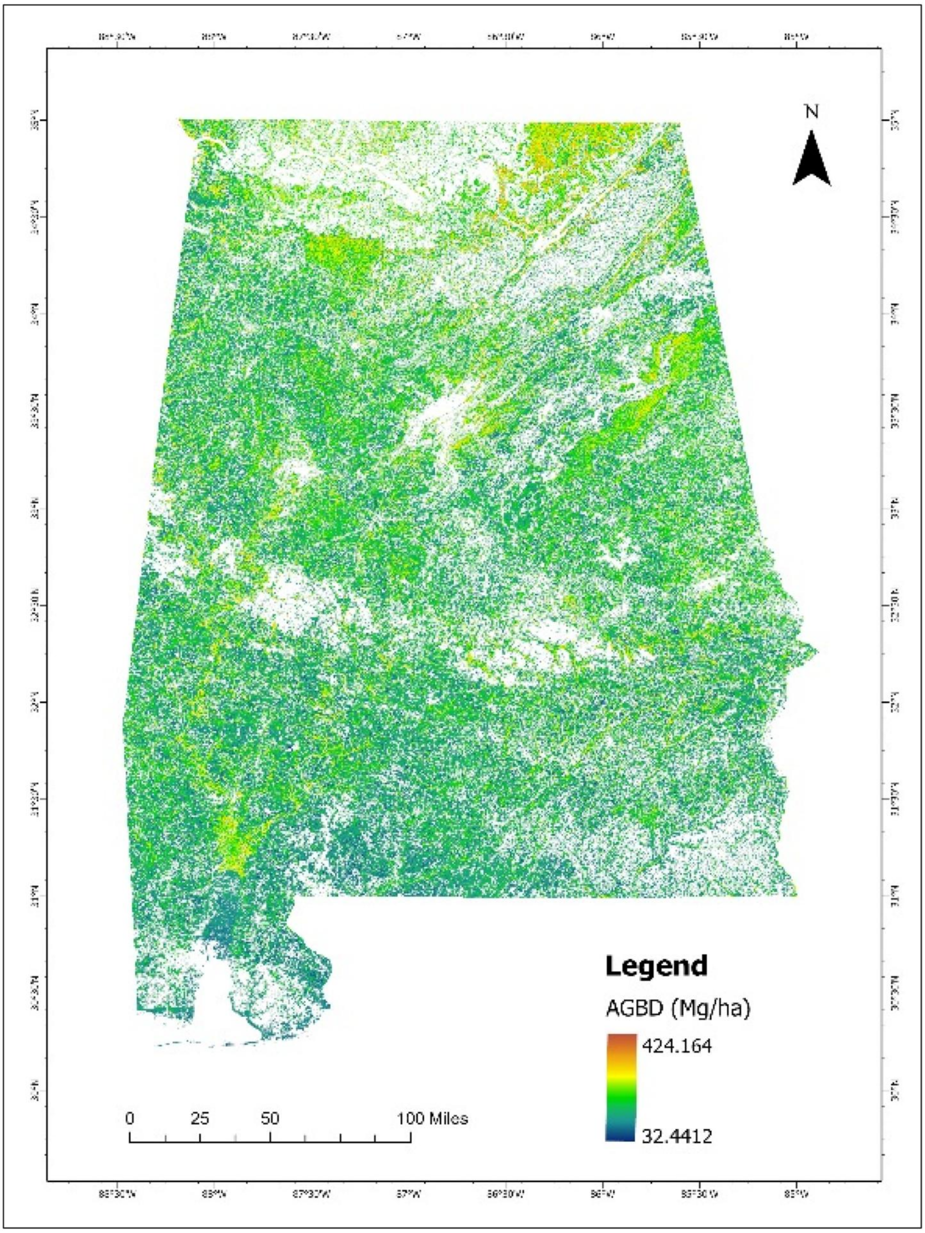

Figure 7. Predicted forest AGBD map for year 2022 at 30 m spatial resolution by ecoregion-specific modeling approach.

terrain metrics (e.g. slope, elevation), SAR predictors (e.g. VV, ratio), and spectral bands like red and SWIR2 play supporting roles in capturing spatial variability in biomass across diverse landscapes. These predictors complement the dominant structural variables by integrating environmental gradients and spectral responses, which provide additional information on vegetation condition, distribution, and biomass accumulation.

The AGBD map in Figure 7 illustrates the 30 m AGB estimates derived from model 2, with an AGBD range of 32.44 Mg/ha to 424.16 Mg/ha. The map reflects spatial variations

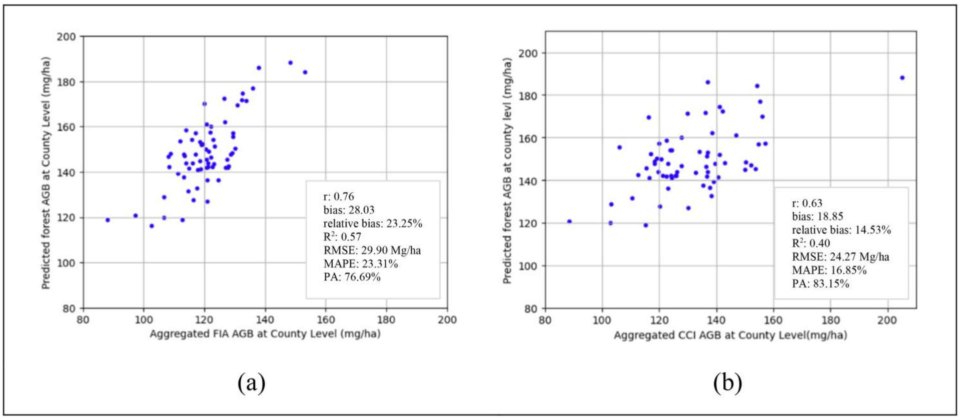

Figure 8. (a) Scatterplot showing the relationship between county-level aggregated mean FIA-derived Forest AGBD and the Forest AGBD estimated in this study. (b) Comparison of county-level aggregated Forest AGBD derived from the CCI product with the mapped Forest AGBD from this study.

in biomass across the state, highlighting differences in vegetation density and structure among ecoregions. The model to predict the highest AGBD value at 424.16 Mg/ha may stem from saturation effects in the lidar-derived GEDI data, where the signal loses sensitivity in densely vegetated regions with high biomass (Li et al. 2024). Additionally, the limited representation of high biomass samples in the training dataset likely influenced the model's predictive performance in this range, as machine learning models tend to underperform when extrapolating beyond the range of observed data. Despite that, the map demonstrates the effectiveness of using ecoregion-specific models to capture biomass variability at a fine spatial resolution. By integrating structural predictors such as LANDFIRE-derived vegetation layers (e.g. EVC, EVH), terrain metrics, and spectral variables, the model provides a spatially explicit and ecologically meaningful representation of AGBD distribution. These results underscore the importance of structural and environmental variables in improving AGBD estimates and highlight the potential of GEDI data combined with EO predictors for regional forest biomass mapping.

3.2. Comparison of mapped AGBD with Forest inventory data and a globally available AGBD product

To demonstrate the applicability of our estimated AGBD, we compared the final output map with FIA data and CCI AGBD products. Since the basis of our analysis is open-source EO data for AGBD estimation, we employed freely available open-access data for this purpose. First, we compared mean AGBD between county-aggregated FIA plot data and estimated AGBD by this study yielded a correlation of 0.76, with a rbias of 23.25%, as illustrated in Figure 8a. Furthermore, county-aggregated CCI AGBD and estimated AGBD by this study yielded a correlation of 0.63, and a rbias of 14.53% as depicted in Figure 8b.

4. Discussion

Spaceborne lidar-derived variables play a crucial role in enhancing the accuracy of mapping the distribution of AGB by capturing forest structural characteristics (Silva et al. 2021). GEDI offers a range of vegetation-related measurements, including AGB, ground elevation, and canopy cover (Dubayah et al. 2022b). These variables have been utilized as either predictors (e.g. GEDI L2A) or response variables (e.g. GEDI L4A) in mapping AGB (Shendryk 2022; Tamiminia et al. 2022; Mohite et al. 2024). Here we implemented GEDI L4A as the response variable in the AGB mapping and incorporated several filtering techniques aimed at enhancing the quality of the footprint AGBD, as recommended by prior research (Kellner et al. 2022; Shendryk 2022; Bruening et al. 2023). Noteworthy is the significant reduction in the GEDI AGBD samples following the filtering process. This underscores the importance of augmenting the number of samples for upscaling AGB, ensuring greater representativeness and accuracy. To address this data loss, future studies could explore methods of data fusion using ICESat-2 and GEDI datasets to enhance data density in canopy height estimation. Such approaches may potentially improve AGBD estimation accuracy.

Utilizing a combination of optical, SAR, and lidar data along with ancillary data as predictor variables, we accessed a substantial range of data for AGB estimation. Studies conducted in forests of the southern US also emphasize the importance of considering a range of variables that capture the high variability of growth patterns in multi-species forests (Brown et al. 2022). For example, Li et al. (2020) demonstrated that the synergy of multiple sensor datasets significantly improves AGB estimates. When combining Landsat-8 and Sentinel-1A data, the model achieved an R^2: $0.20 - 0.71$, and RMSE: 66.67 Mg/ha − 48.99 Mg/ha, outperforming results from using individual datasets. Specifically, using Landsat-8 alone resulted in an R^2 of 0.66 and an RMSE of 20.91 Mg/ha, while Sentinel-1A alone achieved a lower R^2 of 0.38 and an RMSE of 26.79 Mg/ha. This highlights the benefit of integrating optical and SAR data to enhance the accuracy of AGB estimates. Similarly, Liu et al. (2024) reported that integrating Sentinel-2 and environmental data resulted in an R^2 of 0.75 and an RMSE of 23.60 Mg/ha. Their approach incorporated multi-sensor datasets (e.g. Sentinel-1, Sentinel-2, and PALSAR) alongside environmental variables such as climate, topography, soil properties, and disturbance, demonstrating the value of a comprehensive data integration strategy. Consistent with these findings, we incorporated data from a wide range of sources (e.g. Sentinel-1, Sentinel-2, Landsat 9, GLO 30 DEM derivatives, LANDFIRE, and NLCD) related to forest characteristics to effectively capture the complexity of southern mixed forests in AGBD estimation. The majority of data is directly sourced from GEE, obviating the need for manual uploading and processing. This accessibility not only expedites our analytical processes but also capitalizes on GEE's infrastructure, which adeptly manages a larger volume of data through efficient parallel processing across multiple servers.

The implementation of two modeling approaches: one that treated the entire state as a single entity and another that applied an ecoregion-specific strategy highlighted the importance of an ecoregion-specific approach, which led to improved prediction accuracy. Global biomass products like GEDI and CCI provide valuable broader-scale AGB information nevertheless face challenges in capturing finer-scale spatial and temporal variability due to factors such as climate zones, terrain complexity, forest types, and stand density (Bruening et al. 2023; Hunka et al. 2023; Guerra-Hernández et al. 2024). This study highlights the need for an ecoregion-specific approach that accounts for the distinct conditions of each ecological region and emphasizes the importance of regional AGB estimation (Guerra-Hernández et al. 2024). Our ecoregion-specific approach demonstrated notable accuracy and exhibited generalization capabilities, making it applicable to diverse extents within the studied ecoregions.

The RF machine learning algorithm played a key role in this process, given its capability to handle large datasets, account for complex interactions among variables, and produce reliable predictions by aggregating the outputs of multiple decision trees, thereby reducing overfitting and enhancing model performance (Zhang et al. 2014; Shen et al. 2018; Wang et al. 2018; Xu et al. 2023; Wang et al. 2024). RF's consistent superiority over other modeling techniques in AGB mapping has been demonstrated in several studies. For example, Wang et al. (2018) compared various techniques for AGB estimation and reported that the RF model achieved an R^2 of 0.70 and an RMSE of 35.81 Mg/ha, outperforming methods like SVR and MLR. Similarly, Xu et al. (2023) evaluated RF against MLR and SVR, finding that RF provided the most accurate results with an R^2 of 0.91 and an RMSE of 17.93 Mg/ha. Consistent with these findings, our study obtained the highest accuracy an R^2: 0.71 and RMSE: 48.99 Mg/ha for the Ridge and Valley ecoregion among six ecoregions. Moreover, previous AGB mapping efforts that utilized GEDI L4A as a response variable typically achieved spatial resolutions between 100 m and 200 m. Our study advances this by generating a statewide AGBD at 30 m spatial resolution. This resolution enhances the map's utility for ecological and resource management applications by capturing more localized spatial variability in biomass.

The accuracy of our study is influenced by multiple factors related to the complexity of mixed forest structure, characterized by a diverse overstory and understory native to the southern USA (Batista and Platt 1997; Hanberry et al. 2019). These factors present challenges in capturing both spectral and structural diversity, ultimately affecting AGB estimation. Mixed forests, composed of various tree species with different canopy architectures, heights, and foliage densities, create intricate vertical structures that complicate AGB estimation (Brown et al. 2022). The structural complexity introduces shadowing effects in EO data, leading to biases in spectral indexes, indicators, and spectral properties (Freitas et al. 2022). Furthermore, this structural complexity in mixed forests poses challenges for lidar, which may struggle to accurately capture canopy heterogeneity and understory characteristics, thereby reducing model performance (Shao et al. 2018). In addition, the spectral diversity also contributes to the complexity of AGB estimation in mixed forests. The spectral reflectance characteristics of different species vary due to differences in leaf shape, size, pigment concentration, and moisture content (Gates et al. 1965). These variations affect the accuracy of EO-based AGB estimation. Moreover, saturation at high biomass levels, particularly in dense mixed forests in Alabama, limits the ability to estimate AGB effectively with EO data. For example, previous studies have reported saturation values of approximately 159 Mg/ha for pine forests and 152 Mg/ha for mixed forests (Zhao et al. 2016). While lidar is widely employed to mitigate biomass estimation saturation by incorporating structural metrics (e.g. canopy height) as predictor variables (Guo et al. 2008; Mutanga et al. 2023), our study adopts an alternative approach by utilizing spaceborne lidar-derived AGBD (GEDI L4A) as the response variable, with multispectral and SAR datasets as predictors. This inversion of the conventional framework emphasizes the advantages of spaceborne lidar-derived AGBD but there are still challenges when extrapolating wall-to-wall AGBD estimates using other EO datasets. In addition, the heterogeneous nature of southern mixed forests results in mixed pixels, which tend to generalize spatial coverage and fail to capture fine-scale spectral variations unlike pure forest stands (Bolyn et al. 2022). This spectral mixing further complicates the accurate estimation of AGB using remote sensing techniques (Lin et al. 2024). Collectively, these variations reduce the predictive power of the model, thereby affecting the overall accuracy of AGB estimation. Despite these challenges, our estimated AGB achieved a correlation of 0.76 with FIA data, with a rbias of 23.25%, and a correlation of 0.63 with CCI AGBD, with a rbias of 14.53%.

Previous studies have highlighted several limitations of GEDI L4A data in estimating AGBD. For instance, research conducted by Jia et al. (2023) evaluated the accuracy of GEDI L4A using co-registered airborne lidar surveys collected from 2018 to 2019 and corresponding AGBD plots at 19 sites of the National Ecological Observatory Network (NEON). Their analysis revealed that GEDI L4A generally underestimates (e.g. 14 out of the 19 sites) AGBD relative to NEON observations, showing a bias of −31.65 Mg/ha. Additionally, moderate relative errors, ranging from 19% to 50% (%RMSE), were observed at most sites. The study suggests that relying solely on relative heights as predictors in GEDI L4A might limit its ability to account for horizontal structural diversity and the vertical complexity of tree canopies. Furthermore, Bruening et al. (2023) explored discrepancies and outlined precautions regarding GEDI L4A estimates compared to FIA data across the USA. The study highlighted systematic differences between GEDI and FIA estimates, noting overestimations in eastern deciduous forests and underestimations in mixed or predominantly conifer forests in regions such as Maine, the southwestern USA, and the Sierra and Cascade Mountain ranges. The mean difference across hexagons was calculated as −10.48 Mg/ha, with an RMSD of 27.99 Mg/ha. The implementation of the scale-invariant small area (SISA) estimation framework and an enhanced filtering approach significantly reduced bias by 86.7%, with 19.3% attributed to improved filtering and 67.5% to the SISA models. Generally, as previous studies showed AGBD tends to be overestimated at lower levels and underestimated at higher levels (e.g. Shendryk (2022), Jia et al. (2024), Dong et al. (2023)). Since FIA data represents a range of 0 Mg/ha to 160 Mg/ha, this discrepancy might be due to the overestimation of lower AGB values. Despite this, our comparisons showed good correlation and low bias with FIA data (r of 0.76, a rbias of 23.25%). Further, comparisons with the global CCI product yielded moderate correlation and low relative bias (r of 0.63, and rbias of 14.53%). The open source-based validation approach provides valuable insights for future remote sensing endeavors, emphasizing discrepancies among AGB products from various platforms. As a result, it emphasizes the need for continued research to refine methodologies for generating harmonized AGB products (Hunka et al. 2023).

The open-source nature of our data, modeling, and analysis platform highlights the significance of this study in promoting open science. A key advantage of the proposed methodology is its reproducibility and shareability, made possible through GEE, allowing for easy modification and adaptation for AGB estimation. Further research will entail the application of this workflow to assess annual changes in AGBD and the development of a robust monitoring framework. Our findings underscore the critical role of data accessibility, streamlined analysis, and shareability offered by cloud computing platforms like GEE in advancing future AGB estimation efforts.

5. Conclusion

This study presents an ecoregion-based RF modeling framework within a cloud computing platform to map AGBD at a 30 m grid size, using unique characteristics of GEDI L4A data as the response variable while contributing to the growing body of literature on biomass mapping. The results demonstrate that ecoregion-specific models provide improved spatial accuracy and reduced bias compared to a statewide modeling approach, validating the effectiveness of incorporating ecological variability into biomass modeling with GEDI data. Alignment between our AGBD estimates and benchmark datasets, including the CCI AGB maps and FIA data, was observed (FIA data: correlation of 0.76, rbias: 23.25%, and CCI data: correlation 0.63, rbias: 14.53%). Despite these promising findings, limitations remain, particularly regarding underestimation and overestimations, differences in temporal coverage across datasets, and data loss with GEDI filtering. Thus, future studies should explore the integration of additional predictors and extend temporal analyses to improve biomass estimation further. Nevertheless, findings underscore the value of GEDI data for broad-scale forest monitoring and provide a foundation for advancing biomass estimation methodologies in support of global carbon cycle assessments and climate change mitigation strategies.

Acknowledgments

We extend our sincere gratitude to anonymous reviewers, editors, and all members of the College of Forestry, Wildlife, and Environment for their valuable contributions and support.

Author contributions

Conceptualization: JS, LLN; Data curation: JS; Formal analysis: JS; Funding acquisition: LLN; Methodology: JS; Project administration: LLN; Resources: LLN; Software: JS; Supervision: LLN; Validation: JS; Visualization: JS; Writing – original draft: JS; Writing – review & editing: LLN

Disclosure statement

No potential conflict of interest was reported by the author(s).

Funding

This work was carried out at the Geospatial Analytics Laboratory at Auburn University in Auburn, Alabama. The research was funded by the USDA Forest Service (Grant # 22-JV-11330180-064).

Data availability statement

The data used in this study are entirely based on open-access sources. The code is available as a supplementary file.

References

Adjei E, Li W, Narine L, Zhang Y. 2023. What drives land use change in the Southern U.S.? A case study of Alabama. Forests. 14(2):171. [Online], doi: 10.3390/f14020171.

Alabama Forest Commission. 2023. Forest resource report-2023. Montgomery, Alabama.

Almeida CTD, Galvão LS, Aragão LEDOCE, Ometto JPHB, Jacon AD, Pereira FRDS, Sato LY, Lopes AP, Graça PMLDA, Silva CVDJ, et al. 2019. Combining LiDAR and hyperspectral data for aboveground biomass modeling in the Brazilian Amazon using different regression algorithms. Remote Sens Environ. 232:111323. doi: 10.1016/j.rse.2019.111323.

Atkinson AC, Riani M, Corbellini A. 2021. The Box–Cox Transformation: review and Extensions. Statist Sci. 36(2):239–255. 17. doi: 10.1214/20-STS778.

Batista WB, Platt WJ. 1997. An old-growth definition for southern mixed hardwood forests.

Béjar-Martos JA, Rueda-Ruiz AJ, Ogayar-Anguita CJ, Segura-Sánchez RJ, López-Ruiz A. 2022. Strategies for the storage of large LiDAR datasets—a performance comparison. Remote Sensing. 14(11):2623. doi: 10.3390/rs14112623.

Belgiu M, Drăguţ L. 2016. Random forest in remote sensing: a review of applications and future directions. ISPRS J Photogramm Remote Sens. 114:24–31. doi: 10.1016/j.isprsjprs.2016.01.011.

Bhat Y, Kripa MK, Dadhwal VK. 2024. Validation of ESA-CCI forest biomass products over India: methodological and data challenges and results. J Indian Soc Remote Sens. 52(4):931–942. doi: 10.1007/s12524-023-01741-w.

Bolyn C, Lejeune P, Michez A, Latte N. 2022. Mapping tree species proportions from satellite imagery using spectral–spatial deep learning. Remote Sens Environ. 280:113205. doi: 10.1016/j.rse.2022.113205.

Bouasria A, Bouslihim Y, Gupta S, Taghizadeh-Mehrjardi R, Hengl T. 2023. Predictive performance of machine learning model with varying sampling designs, sample sizes, and spatial extents. Ecol Inf. 78:102294. doi: 10.1016/j.ecoinf.2023.102294.

Brown S, Narine LL, Gilbert J. 2022. Using airborne lidar, multispectral imagery, and field inventory data to estimate basal area, volume, and aboveground biomass in heterogeneous mixed species forests: a case study in Southern Alabama. Remote Sensing. 14(11):2708. doi: 10.3390/rs14112708.

Bruening J, May P, Armston J, Dubayah R. 2023. Precise and unbiased biomass estimation from GEDI data and the US forest inventory. Front For Glob Change. 6:1149153. doi: 10.3389/ffgc.2023.1149153.

Chen J, Chen J, Liao A, Cao X, Chen L, Chen X, He C, Han G, Peng S, Lu M, et al. 2015. Global land cover mapping at 30m resolution: a POK-based operational approach. ISPRS J Photogramm Remote Sens. 103:7–27. doi: 10.1016/j.isprsjprs.2014.09.002.

Chen L, Wang Y, Ren C, Zhang B, Wang Z. 2019. Optimal combination of predictors and algorithms for forest above-ground biomass mapping from Sentinel and SRTM data. Remote Sensing. 11(4):414. [Online] doi: 10.3390/rs11040414.

Chen X. 2010. Trends of forest inventory data in Alabama, USA, during the last seven decades. Forestry. 83(5):517–526. doi: 10.1093/forestry/cpq034.

Commission for Environmental Cooperation (Montréal, Québec), & Secretariat. 1997. Ecological regions of North America: toward a common perspective. Canada: Commission for Environmental Cooperation.

Dewitz J. 2023. National land cover database (NLCD) 2021 products. USGS Asset Identifier Service (AIS) USGS Organization: Earth Resources Observation and Science (EROS) Center. doi: 10.5066/P9JZ7AO3.

Dong W, Mitchard ETA, Yu H, Hancock S, Ryan CM. 2023. Forest aboveground biomass estimation using GEDI and earth observation data through attention-based deep learning. arXiv preprint arXiv:2311.03067.

Dubayah R, Armston J, Healey SP, Bruening JM, Patterson PL, Kellner JR, Duncanson L, Saarela S, Ståhl G, Yang Z, et al. 2022a. GEDI launches a new era of biomass inference from space. Environ Res Lett. 17(9):095001. doi: 10.1088/1748-9326/ac8694.

Dubayah R, Bryan J, Goetz S, Fatoyinbo L, Hansen M, Healey S, Hofton M, Hurtt G, Kellner J, Luthcke S, et al. 2020. The Global Ecosystem Dynamics Investigation: high-resolution laser ranging of the Earth's forests and topography. Sci Remote Sens. 1:100002. doi: 10.1016/j.srs.2020.100002.

Dubayah RO, Armston J, Healey SP, Yang Z, Patterson PL, Saarela S, Stahl G, Duncanson L, Kellner JR, Bruening J, et al. 2023. GEDI L4B gridded aboveground biomass density, version 2. Oak Ridge (TN): ORNL DAAC.

Dubayah RO, Armston J, Kellner JR, Duncanson L, Healey SP, Patterson PL, Hancock S, Tang H, Bruening J, Hofton MA, et al. 2022b. GEDI L4A footprint level aboveground biomass density, version 2.1. Oak Ridge (TN): ORNL DAAC.

Duncan RS. 2013. Encyclopedia of Alabama [Online]. [accessed 2024 Jan 19]. Available from: https://encyclopediaofalabama.org/article/biodiversity-in-alabama/

ESA. 2012. Sentinel-1. In: Fletcher, K, editor. Sentinel-1: ESA's radar observatory mission for GMES operational services. Netherlands: European Space Agency.

ESA. 2022. STEP - Scientific Toolbox Exploitation Platform [Online]. European Space Agency. [accessed 2024 Jan 31]. Available from: https://step.esa.int/main/snap-supported-plugins/sen2cor/

ESRI. 2024. ArcGIS Pro (Version 3.2) ed. Redlands, CA: Environmental Systems Research Institute, Inc.

Franks S, Rengarajan R. 2023. Evaluation of Copernicus DEM and comparison to the DEM used for Landsat collection-2 processing. Remote Sens. 15(10):2509. doi: 10.3390/rs15102509.

Freeman EA, Frescino TS, Moisen GG. 2018. ModelMap: an R package for model creation and map production. R Package Version. 4:6–12.

Freitas P, Vieira G, Mora C, Canário J, Vincent WF. 2022. Vegetation shadow casts impact remotely sensed reflectance from permafrost thaw ponds in the subarctic forest-tundra zone. Environ Earth Sci. 81(22):522. doi: 10.1007/s12665-022-10640-1.

Gates DM, Keegan HJ, Schleter JC, Weidner VR. 1965. Spectral properties of plants. Appl Opt. 4(1):11–20. doi: 10.1364/AO.4.000011.

Giri C, Pengra B, Long J, Loveland TR. 2013. Next generation of global land cover characterization, mapping, and monitoring. Int J Appl Earth Obs Geoinf. 25:30–37. doi: 10.1016/j.jag.2013.03.005.

Gitelson AA, Merzlyak MN. 1998. Remote sensing of chlorophyll concentration in higher plant leaves. Adv Space Res. 22(5):689–692. doi: 10.1016/S0273-1177(97)01133-2.

Gitelson AA, Viña A, Ciganda V, Rundquist DC, Arkebauer TJ. 2005. Remote estimation of canopy chlorophyll content in crops. Geophys Res Lett. 32(8):L08403. doi: 10.1029/2005GL022688.

Gorelick N, Hancher M, Dixon M, Ilyushchenko S, Thau D, Moore R. 2017. Google Earth Engine: planetary-scale geospatial analysis for everyone. Remote Sens Environ. 202:18–27. doi: 10.1016/j.rse.2017.06.031.

Gray AN, Brandeis TJ, Shaw JD, McWilliams WH, Miles PD. (2012). Forest inventory and analysis database of the United States of America (FIA). In Dengler J, Oldeland J, Jansen F, Chytrý M, Ewald J, Finckh M, Glöckler F, Lopez-Gonzalez G, Peet RK, Schaminée JHJ, editor. Vegetation databases for the 21st century. Biodiversity & Ecology 4: 225–231. doi: 10.7809/b-e.00079.

Gregoire TG, Lin QF, Boudreau J, Nelson R. 2008. Regression estimation following the square-root transformation of the response. Forest Sci. 54(6):597–606. doi: 10.1093/forestscience/54.6.597.
Guerra-Hernández J, Narine LL, Pascual A, Gonzalez-Ferreiro E, Botequim B, Malambo L, Neuenschwander A, Popescu SC, Godinho S. 2022. Aboveground biomass mapping by integrating ICESat-2, SENTINEL-1, SENTINEL-2, ALOS2/PALSAR2, and topographic information in Mediterranean forests. GIScience Remote Sens. 59(1):1509–1533. doi: 10.1080/15481603.2022.2115599.
Guerra-Hernández J, Pascual A, Tupinambá-Simões F, Godinho S, Botequim B, Jurado-Varela A, Sandoval-Altelarrea V. 2024. Using bi-temporal ALS and NFI-based time-series data to account for large-scale aboveground carbon dynamics: the showcase of mediterranean forests. Eur J Remote Sens. 57(1):2315413. doi: 10.1080/22797254.2024.2315413.
Guo Z, Sun G, Ranson KJ, Ni W, Qin W. 2008. The potential of combined Lidar and SAR data in retrieving forest parameters using model analysis. In: IGARSS 2008 - 2008 IEEE International Geoscience and Remote Sensing Symposium, Jul 7–11; p. V-542–V-545. doi: 10.1109/IGARSS.2008.4780149.
Hanberry BB, Brzuszek RF, Foster HT, II, Schauwecker TJ. 2019. Recalling open old growth forests in the Southeastern Mixed Forest province of the United States. Écoscience. 26(1):11–22. doi: 10.1080/11956860.2018.1499282.
Hansen MC, Potapov PV, Moore R, Hancher M, Turubanova SA, Tyukavina A, Thau D, Stehman SV, Goetz SJ, Loveland TR, et al. 2013. High-resolution global maps of 21st-century forest cover change. Science. 342(6160):850–853. doi: 10.1126/science.1244693.
Harris NL, Gibbs DA, Baccini A, Birdsey RA, DE Bruin S, Farina M, Fatoyinbo L, Hansen MC, Herold M, Houghton RA, et al. 2021. Global maps of twenty-first century forest carbon fluxes. Nat Clim Change. 11(3):234–240. doi: 10.1038/s41558-020-00976-6.
Hartsell AJ, Cooper JA. 2013. Alabama's forests, 2010. Resour. Bull. SRS-RB-193. Asheville (NC): US Department of Agriculture Forest Service, Southern Research Station. 87 p., 193; p. 1–87.
Holcomb A, Mathis SV, Coomes DA, Keshav S. 2023. Computational tools for assessing forest recovery with GEDI shots and forest change maps. Science of Remote Sensing. 8:100106. doi: 10.1016/j.srs.2023.100106.
Huete AR. 1988. A soil-adjusted vegetation index (SAVI). Remote Sens Environ. 25(3):295–309. doi: 10.1016/0034-4257(88)90106-X.
Hummel S, Hudak AT, Uebler EH, Falkowski M, Megown K. 2011. A comparison of accuracy and cost of LiDAR versus stand exam data for landscape management on the Malheur National Forest. J For. 109(5):267–273. doi: 10.1093/jof/109.5.267.
Hunka N, Santoro M, Armston J, Dubayah R, Mcroberts RE, Næsset E, Quegan S, Urbazaev M, Pascual A, May PB, et al. 2023. On the NASA GEDI and ESA CCI biomass maps: aligning for uptake in the UNFCCC global stocktake. Environ Res Lett. 18(12):124042. doi: 10.1088/1748-9326/ad0b60.
Indirabai I, Nilsson M. 2024. Estimation of above ground biomass in tropical heterogeneous forests in India using GEDI. Ecol Inf. 82:102712. doi: 10.1016/j.ecoinf.2024.102712.
Jia D, Wang C, Hakkenberg CR, Numata I, Elmore AJ, Cochrane MA. 2023. Accuracy evaluation and effect factor analysis of GEDI aboveground biomass product for temperate forests in the conterminous United States. GIScience Remote Sens. 61(1):2292374. doi: 10.1080/15481603.2023.2292374.
Jiang F, Sun H, Chen E, Wang T, Cao Y, Liu Q. 2022. Above-ground biomass estimation for coniferous forests in Northern China using regression kriging and Landsat 9 images. Remote Sensing. 14(22):5734. [Online] doi: 10.3390/rs14225734.
Jordan CF. 1969. Derivation of leaf-area index from quality of light on the forest floor. Ecology. 50(4):663–666. doi: 10.2307/1936256.
Kacic P, Hirner A, DA Ponte E. 2021. Fusing Sentinel-1 and -2 to model GEDI-derived vegetation structure characteristics in GEE for the Paraguayan Chaco. Remote Sensing. 13(24):5105. doi: 10.3390/rs13245105.
Kellner JR, Armston J, Duncanson L. 2022. Algorithm theoretical basis document for GEDI footprint aboveground biomass density. Earth Space Sci. 10:1–20.
Kristi Sayler TG. 2022. Landsat 9 data users handbook (LSDs-2082, Version 1.0). Department of the Interior U.S. Geological Survey. Sioux Falls, South Dakota: USGS Earth Resources Observation and Science (EROS) Center.
La Puma IP. 2023. LANDFIRE technical documentation: U.S. Geological Survey Open-File Report 2023-1045, p. 103. doi: 10.3133/ofr20231045.
Laurin GV, Balling J, Corona P, Mattioli W, Papale D, Puletti N, Rizzo M, Truckenbrodt J, Urban M. 2018. Above-ground biomass prediction by Sentinel-1 multitemporal data in central Italy with integration of ALOS2 and Sentinel-2 data. J Appl Rem Sens. 12(01):1–1. doi: 10.1117/1.JRS.12.016008.
Leydesdorff L, Bensman S. 2006. Classification and powerlaws: The logarithmic transformation. J Am Soc Inf Sci. 57(11):1470–1486. doi: 10.1002/asi.20467.

Li H, Li X, Kato T, Hayashi M, Fu J, Hiroshima T. 2024. Accuracy assessment of GEDI terrain elevation, canopy height, and aboveground biomass density estimates in Japanese artificial forests. Sci Remote Sens. 10:100144. doi: 10.1016/j.srs.2024.100144.

Li Y, Li M, Li C, Liu Z. 2020. Forest aboveground biomass estimation using Landsat 8 and Sentinel-1A data with machine learning algorithms. Sci Rep. 10(1):9952. doi: 10.1038/s41598-020-67024-3.

Lin Z, Cheng KH, Yang D, Xu F, Song G, Meng R, Wang J, Zhu X, Ng M, Wu J. 2024. Ecoregion-wise fractional mapping of tree functional composition in temperate mixed forests with sentinel data: integrating time-series spectral and radar data. Remote Sens Environ. 304:114026. doi: 10.1016/j.rse.2024.114026.

Liu A, Cheng X, Chen Z. 2021. Performance evaluation of GEDI and ICESat-2 laser altimeter data for terrain and canopy height retrievals. Remote Sens Environ. 264:112571. doi: 10.1016/j.rse.2021.112571.

Liu P, Ren C, Yang X, Wang Z, Jia M, Zhao C, Yu W, Ren H. 2024. Combining Sentinel-2 and diverse environmental data largely improved aboveground biomass estimation in China's boreal forests. Sci Rep. 14(1):27528. doi: 10.1038/s41598-024-78615-9.

Lutz N, Rodriguez-Veiga P, Menor IO. 2024. Estimating vegetation structure and aboveground carbon storage in Western Australia using GEDI LiDAR, Landsat and Sentinel data. Environ Res: Ecol. 3(4): 045004. doi: 10.1088/2752-664X/ad7f5a.

Malambo L, Popescu S, Liu M. 2023. Landsat-scale regional forest canopy height mapping using ICESat-2 along-track heights: case study of eastern Texas. Remote Sensing. 15(1):1. doi: 10.3390/rs15010001.

Masek JG, Wulder MA, Markham B, Mccorkel J, Crawford CJ, Storey J, Jenstrom DT. 2020. Landsat 9: Empowering open science and applications through continuity. Remote Sens Environ. 248:111968. doi: 10.1016/j.rse.2020.111968.

Mohite J, Sawant S, Pandit A, Sakkan M, Pappula S, Parmar A. 2024. Forest aboveground biomass estimation by GEDI and multi-source EO data fusion over Indian forest. Int J Remote Sens. 45(4):1304–1338. doi: 10.1080/01431161.2024.2307944.

Moradi F, Darvishsefat AA, Pourrahmati MR, Deljouei A, Borz SA. 2022. Estimating aboveground biomass in dense Hyrcanian forests by the use of Sentinel-2 data. Forests. 13(1):104. doi: 10.3390/f13010104.

Mutanga O, Masenyama A, Sibanda M. 2023. Spectral saturation in the remote sensing of high-density vegetation traits: a systematic review of progress, challenges, and prospects. ISPRS J Photogramm Remote Sens. 198:297–309. doi: 10.1016/j.isprsjprs.2023.03.010.

Nandy S, Srinet R, Padalia H. 2021. Mapping forest height and aboveground biomass by integrating ICESat-2, Sentinel-1 and Sentinel-2 data using random forest algorithm in northwest Himalayan foothills of India. Geophys Res Lett. 48(14):1–10. doi: 10.1029/2021GL093799.

Narine LL, Popescu SC, Malambo L. 2019. Synergy of ICESat-2 and Landsat for mapping forest aboveground biomass with deep learning. Remote Sen. 11(12):1503. doi: 10.3390/rs11121503.

Planet Labs. 2024. Forest carbon monitoring technical specification [Online]. Planet Labs PBC. [accessed 2024 Dec 23]. Available from: https://developers.planet.com/docs/planetary-variables/forest-carbon-monitoring-technical-specification/

Qi J, Chehbouni A, Huete AR, Kerr YH, Sorooshian S. 1994. A modified soil adjusted vegetation index. Remote Sens Environ. 48(2):119–126. doi: 10.1016/0034-4257(94)90134-1.

Rodríguez-Veiga P, Wheeler J, Louis V, Tansey K, Balzter H. 2017. Quantifying forest biomass carbon stocks from space. Curr For Rep. 3(1):1–18. doi: 10.1007/s40725-017-0052-5.

Roitman I, Bustamante MMC, Haidar RF, Shimbo JZ, Abdala GC, Eiten G, Fagg CW, Felfili MC, Felfili JM, Jacobson TKB, et al. 2018. Optimizing biomass estimates of savanna woodland at different spatial scales in the Brazilian Cerrado: re-evaluating allometric equations and environmental influences. PLoS One. 13(8):e0196742. doi: 10.1371/journal.pone.0196742.

Rollins MG. 2009. LANDFIRE: a nationally consistent vegetation, wildland fire, and fuel assessment. Int J Wildland Fire. 18(3):235–249. doi: 10.1071/WF08088.

Rondeaux G, Steven M, Baret F. 1996. Optimization of soil-adjusted vegetation indices. Remote Sens Environ. 55(2):95–107. doi: 10.1016/0034-4257(95)00186-7.

Ross S. 2013. Chapter 5 - Generating continuous random variables. In: Ross, S, editor. Simulation. 5th ed. Elsevier, New York: Academic Press.

Rouse JW, Haas RH, Schell JA, Deering DW. 1974. Monitoring vegetation systems in the great plains with ERTS. In: Freden SC, Mercanti EP, Becker MA. editors. NASA Special Publication (Vol. 351, p. 309). https://ui.adsabs.harvard.edu/abs/1974NASSP.351..309R

Santoro M, Cartus O. 2023. ESA Biomass Climate Change Initiative (Biomass_cci): Global datasets of forest above-ground biomass for the years 2010, 2017, 2018, 2019 and 2020, v4. NERC EDS Centre for Environmental Data Analysis, 21 April 2023. doi: 10.5285/af60720c1e404a9e9d2c145d2b2ead4e.

Shao G, Shao G, Gallion J, Saunders MR, Frankenberger JR, Fei S. 2018. Improving Lidar-based aboveground biomass estimation of temperate hardwood forests with varying site productivity. Remote Sens Environ. 204:872–882. doi: 10.1016/j.rse.2017.09.011.

Shen W, Li M, Huang C, Tao X, Wei A. 2018. Annual forest aboveground biomass changes mapped using ICESat/GLAS measurements, historical inventory data, and time-series optical and radar imagery for Guangdong province, China. Agric For Meteorol. 259:23–38. doi: 10.1016/j.agrformet.2018.04.005.

Shendryk Y. 2022. Fusing GEDI with earth observation data for large area aboveground biomass mapping. Int J Appl Earth Obs Geoinf. 115:103108–103108. doi: 10.1016/j.jag.2022.103108.

Shephard NT, Narine L, Peng Y, Maggard A. 2022. Climate smart forestry in the Southern United States. Forests. 13(9):1460. [Online], doi: 10.3390/f13091460.

Silva CA, Duncanson L, Hancock S, Neuenschwander A, Thomas N, Hofton M, Fatoyinbo L, Simard M, Marshak CZ, Armston J, et al. 2021. Fusing simulated GEDI, ICESat-2 and NISAR data for regional aboveground biomass mapping. Remote Sens Environ. 253:112234. doi: 10.1016/j.rse.2020.112234.

Soudani K, Delpierre N, Berveiller D, Hmimina G, Vincent G, Morfin A, Dufrêne É. 2021. Potential of C-band Synthetic Aperture Radar Sentinel-1 time-series for the monitoring of phenological cycles in a deciduous forest. Int J Appl Earth Obs Geoinf. 104:102505. doi: 10.1016/j.jag.2021.102505.

Su H, Shen W, Wang J, Ali A, Li M. 2020. Machine learning and geostatistical approaches for estimating aboveground biomass in Chinese subtropical forests. For Ecosyst. 7(1):64. doi: 10.1186/s40663-020-00276-7.

Tamiminia H, Salehi B, Mahdianpari M, Beier CM, Johnson L. 2022. Mapping two decades of New York State Forest aboveground biomass change using remote sensing. Remote Sensing. 14(16):4097. [Online], doi: 10.3390/rs14164097.

Tiwari K, Narine LL. 2022. A comparison of machine learning and geostatistical approaches for mapping forest canopy height over the southeastern US using ICESat-2. Remote Sens. 14(22):5651. doi: 10.3390/rs14225651.

Townshend JR, Masek JG, Huang C, Vermote EF, Gao F, Channan S, Sexton JO, Feng M, Narasimhan R, Kim D, et al. 2012. Global characterization and monitoring of forest cover using Landsat data: opportunities and challenges. Int J Digital Earth. 5(5):373–397. doi: 10.1080/17538947.2012.713190.

USFWI. 2024. Alabama Butterfly Atlas [Online]. Tampa, FL, USA: University of South Florida Water Institute Publisher. https://alabama.butterflyatlas.usf.edu/geographic-regions

USGS. 2024. What are the best Landsat spectral bands to use for my research? [Online]. Department of the Interior. [accessed 2024 Dec 23]. Available from: https://www.usgs.gov/faqs/what-are-best-landsat-spectral-bands-use-my-research

Van Do T, Yamamoto M, Kozan O, Hai, VD, Trung PD, Thang NT, Hai LT, Nam VT, Hung TT, Van Thang H, Manh, et al. 2020. Ecoregional variations of aboveground biomass and stand structure in evergreen broadleaved forests. J For Res. 31(5):1713–1722. doi: 10.1007/s11676-019-00969-y.

Wang C, Zhang W, Ji Y, Marino A, Li C, Wang L, Zhao H, Wang M. 2024. Estimation of aboveground biomass for different forest types using data from Sentinel-1, Sentinel-2, ALOS PALSAR-2, and GEDI. Forests,. 15(1):215. doi: 10.3390/f15010215.

Wang M, Sun R, Xiao Z. 2018. Estimation of forest canopy height and aboveground biomass from spaceborne LiDAR and Landsat imageries in Maryland. Remote Sens. 10(2):344. doi: 10.3390/rs10020344.

Xu L, Shu Q, Fu H, Zhou W, Luo S, Gao Y, Yu J, Guo C, Yang Z, Xiao J, et al. 2023. Estimation of Quercus biomass in Shangri-La based on GEDI spaceborne Lidar data. Forests. 14(5):876. doi: 10.3390/f14050876.

Yang Q, Niu C, Liu X, Feng Y, Ma Q, Wang X, Tang H, Guo Q. 2023. Mapping high-resolution forest aboveground biomass of China using multisource remote sensing data. GIScience Remote Sens. 60(1): 2203303. doi: 10.1080/15481603.2023.2203303.

Zhang J, Huang S, Hogg EH, Lieffers V, Qin Y, He F. 2014. Estimating spatial variation in Alberta forest biomass from a combination of forest inventory and remote sensing data. Biogeosciences. 11(10):2793–2808. doi: 10.5194/bg-11-2793-2014.

Zhang X, Friedl MA, Schaaf CB, Strahler AH, Hodges JCF, Gao F, Reed BC, Huete A. 2003. Monitoring vegetation phenology using MODIS. Remote Sens Environ. 84(3):471–475. doi: 10.1016/S0034-4257(02)00135-9.

Zhao P, Lu D, Wang G, Wu C, Huang Y, Yu S. 2016. Examining spectral reflectance saturation in Landsat imagery and corresponding solutions to improve forest aboveground biomass estimation. Remote Sens. 8(6):469. doi: 10.3390/rs8060469.